Geometric and Electronic Structures for MnS 2 −/0 Clusters by Interpreting the Anion Photoelectron Spectrum with Quantum Chemical Calculations

ARTICLE *in* THE JOURNAL OF PHYSICAL CHEMISTRY A · MAY 2015

Impact Factor: 2.69 · DOI: 10.1021/acs.jpca.5b02896 · Source: PubMed

3 AUTHORS:

Van Tan Tran

chemistry

15 PUBLICATIONS **96** CITATIONS

SEE PROFILE

Quoc Tri Tran

Dong Thap University

4 PUBLICATIONS **8** CITATIONS

SEE PROFILE

Marc F A Hendrickx

University of Leuven

28 PUBLICATIONS **248** CITATIONS

SEE PROFILE

THE JOURNAL OF PHYSICAL CHEMISTRY A

Article

pubs.acs.org/JPCA

Geometric and Electronic Structures for $MnS_2^{-/0}$ Clusters by Interpreting the Anion Photoelectron Spectrum with Quantum Chemical Calculations

Van Tan Tran,[†] Quoc Tri Tran,[†] and Marc F. A. Hendrickx*[,‡]

[†]Theoretical and Physical Chemistry Division, Dong Thap University, 783-Pham Huu Lau, Cao Lanh City, Dong Thap Vietnam

[‡]Afdeling Kwantumchemie en Fysicochemie, Departement Chemie, Katholieke Universiteit Leuven, Celestijnenlaan 200F, B-3001 Heverlee-Leuven, Belgium

ABSTRACT: Geometric and electronic structures of linear SMnS, cyclic η^2-MnS_2, and linear η^1-MnS_2 isomers of MnS_2^- clusters have been investigated with B3LYP, CCSD(T), and NEVPT2 methods. The ground state of the anionic cluster is determined as $^5\Pi_g$ of the linear $SMnS^-$ isomer, while the ground state of the neutral cluster may be either the $^4\Sigma_g^-$ of the same isomer or the $^6A_1$ of the η^2-MnS_2 cluster. The experimental photoelectron spectrum of the MnS_2^- cluster is interpreted by contributions of these two isomers. The high-intensity band at a binding energy of 2.94 eV is attributed to the $^5\Pi_g \rightarrow {}^4\Sigma_g^-$ transition between the linear $SMnS^{-/0}$ clusters. The lower energy feature in the spectrum at binding energies between 1.9 and 2.8 eV and exhibiting a low intensity, is ascribed to electron detachments within the less stable η^2-$MnS_2^{-/0}$ clusters. Ionizations from the lowest energy $^7A_1$ state of this isomer to the neutral $^6A_1$, $^6A_2$, $^8A_2$, and $^6B_2$ states are responsible for this part of the spectrum. The extreme low intensity part between 1.3 and 1.9 eV can be due to excited states of either $SMnS^-$ or η^2-MnS_2^-.

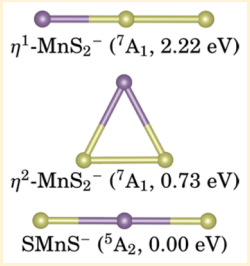

INTRODUCTION

The geometric and electronic structures of small-sized transition metal−sulfur clusters have been extensively investigated with both experimental and computational methods, due to the fact they can serve as models to understand biological and industrial catalysis and the properties of related bulk materials.[1−15] In particular, these types of clusters are usually studied by matrix-isolation infrared[3−7] and photoelectron spectroscopy,[8−10] while quantum chemical calculations are performed in order to understand the geometric and electronic structures by the assignments for their spectra.[11−15] In this work, the $MnS_2^{-/0}$ clusters are investigated, for which the anion photoelectron spectrum was reported many years ago but, rather curiously, has not been understood fully yet.[10,16] The spectrum, as measured at photon energy of 355 nm, shows two features with very different intensities.[10] The higher energy band with the highest intensity at 2.94 eV was attributed to an electron detachment of the rigid SMnS isomer, which contains two S moieties bound to Mn.[10] This assignment for the second band was later confirmed by density functional calculations.[16] On the other hand, the first broad feature ranging from 1.30 to 2.80 eV with considerably lower intensity was thought to be the result of several electron detachments within the flexible η^2-MnS_2 isomer, in which a S_2 ligand binds side-on to Mn.[10] This proposed assignment for the first band has to-date not been confirmed at any quantum chemical computational level.

The $MnS_2^{-/0}$ clusters are expected to possess complicated electronic structures as is usually the case for compounds exhibiting an open 3d shell system on the transition metal center. Indeed, computations on similar type of complexes show several nearly degenerate low-lying electronic states and almost equal stabilities of different isomers for a particular stoichiometry.[13,14,17−19] For this reason reliable investigations into the nature of transition metal-containing sulfur clusters must be carried out with high-accurate quantum chemical methods. However, the most commonly applied computational methods on this class of clusters are density functional theory (DFT) techniques, chosen mainly because of their low computational cost. Moreover, for the purpose of reaching a dependable description of the multireference properties of the wave functions, CASPT2 (complete active space second-order perturbation theory) was used. On the other hand, NEVPT2 (N-electron valence state perturbation theory), which employs a different zeroth-order Hamiltonian (the Dyall Hamiltonian) than CASPT2 and is free of intruder states, has also been successfully applied to investigate transition metal-containing clusters.[20−28] Further, for electronic states with a sufficient single reference character, CCSD(T) (coupled-cluster with single and double and perturbative triple excitations), with its supreme ability to recover dynamical correlation energy, has been utilized fruitfully on transition metal−sulfur clusters in order to get the correct estimation of the relative energy order of closely positioned electronic states and isomers.[13,14] In this work, DFT, CCSD(T), and NEVPT2 methods will be used to investigate the complicated geometric and electronic structures of $MnS_2^{-/0}$ clusters in an effort to explain all features in the corresponding experimental anion photoelectron spectrum.

Received: March 26, 2015
Revised: May 13, 2015

DOI: 10.1021/acs.jpca.5b02896
J. Phys. Chem. A XXXX, XXX, XXX−XXX

COMPUTATIONAL METHODS

All three possible isomers of the studied clusters as depicted in Figure 1, were explored by calculating all low-lying electronic states. A first isomer will be denoted as $SMnS^{-/0}$ which contains two individual atomic S moieties bound to the central Mn atom (Figure 1a). The second and third isomers are the cyclic η^2-$MnS_2^{-/0}$ (Figure 1b) and the linear η^1-$MnS_2^{-/0}$ (Figure 1c), which are formed by a side-on and end-on binding of an S_2 entity to the Mn atom, respectively. All computations for these isomers were done within the C_{2v} point group using the coordinate systems as depicted in Figure 1.

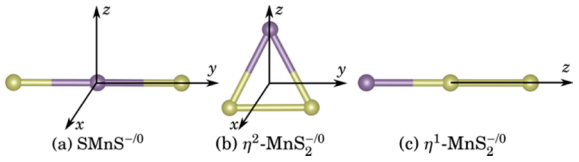

Figure 1. Three isomers for the $MnS_2^{-/0}$ clusters studied in this work and the corresponding coordinate systems. The Mn atom is positioned in the middle of the linear $SMnS^-$, on the top of η^2-$MnS_2^{-/0}$, and on the left-hand side of the η^1-$MnS_2^{-/0}$.

A combination of single-reference DFT, CCSD(T), and multireference NEVPT2 methods was utilized in our computational study. For DFT calculations, previous results on $FeS_n^{-/0}$ (n = 1−4) show that B3LYP[29−31] is the better functional for sulfur-containing clusters and therefore this functional is used to study the title $MnS_2^{-/0}$ clusters.[11−14] Unrestricted DFT were carried out with 6-311++G(3df,3pd) basis set for both Mn and S atoms.[32,33] Geometries of the different low-lying electronic states of three isomers of $MnS_2^{-/0}$ clusters were optimized. Harmonic vibrational frequency calculations were performed to ensure that the found geometries are true minima on the potential energy surface. Based on the B3LYP geometries, single point ROHF/CCSD(T) calculations were performed in order to improve the relative energies. The aug-cc-pwCVTZ-DK[34] and aug-cc-pVTZ-DK[35] basis sets are employed for Mn and S, respectively. In addition to all the valence electrons, the outer core electrons of Mn (3s and 3p electrons) were correlated. Scalar-relativistic effects were included in CCSD(T) through the second-order Douglas−Kroll Hamiltonian.[36−38] All DFT calculations were performed with the ORCA package,[39] while ROHF/CCSD(T) calculations were performed with the NWCHEM computational chemistry code.[40]

With the purpose to obtain zero-order wave functions for NEVPT2, CASSCF calculations were performed with an active space of 15 or 16 electrons in 13 orbitals. This active space was constructed by including the 3d and 4s orbitals of Mn, the 3p orbitals of S, and one virtual orbital of the total symmetric irreducible representation, in order to increase its flexibility. The aug-cc-pVTZ-DK basis set[34,35] was utilized for both Mn and S. All outer core electrons of Mn (3s and 3p electrons) and the 3s of S were additionally correlated in the succeeding NEVPT2 step of the calculations. Scalar-relativistic effects were included through the second-order Douglas−Kroll Hamiltonian.[36−38] As a multireference technique, NEVPT2 is particularly well suited for identifying the nature of the low-lying open shell electronic states by calculating all potential important spin multiplicities for all of the four irreducible representations of the C_{2v} point group. Further, equilibrium structures of the lowest electronic states of the $MnS_2^{-/0}$ isomers were located by exploring the potential energy hypersurfaces at this multireference level. More specifically, potential energy profiles for the spectroscopically important states were constructed manually by symmetrically stretching the Mn−S

Table 1. Geometric Parameters, Vibrational Frequencies, and Adiabatic Relative Energies (ARE) of Low-Lying Electronic States of Different Isomers of $MnS_2^{-/0}$ Clusters As Calculated at the B3LYP and CCSD(T) Levels

method	cluster	state	Mn−S (Å), SMnS (deg), S−S (Å)	frequencies (cm^{-1})[a]	ARE (eV)[c]
B3LYP	$SMnS^-$	$^5A_2$ ($^5\Pi_g$)	2.177, 179.13	89, 329, 439	0.00
		$^5B_2$ ($^5\Pi_g$)	2.177, 179.00	44, 329, 439	0.00
	SMnS	$^4B_1$	2.075, 136.70	56, 370, 444	3.12
	η^2-MnS_2^-	$^7A_1$	2.350, 55.25	263, 299, 444	1.00 (0.00)
		$^5A_1$	2.323, 56.27	242, 297, 440	1.43 (0.43)
	η^2-MnS_2	$^6A_1$	2.216, 60.29	293, 318, 467	2.96 (1.96)
		$^6A_2$	2.467, 48.24	270, 374, 588	3.22 (2.22)
		$^8A_2$	2.489, 47.80	216, 273, 575	3.23 (2.23)
		$^6B_2$	2.385, 50.41	254, 260, 560	3.67 (2.67)
	η^1-MnS_2^-	$^7A_1$ ($^7\Sigma^+$)	2.156, 180.00, 2.054	296, 365(x2), 571	2.20
	η^1-MnS_2	$^6B_1$ ($^6\Pi$)	2.239, 180.00, 1.973	271, 391(x2), 616	4.20
CCSD(T)[b]	$SMnS^-$	$^5A_2$			0.00
		$^5B_2$			0.00
	SMnS	$^4B_1$			3.07
	η^2-MnS_2^-	$^7A_1$			0.73 (0.00)
	η^2-MnS_2	$^6A_1$			3.01 (2.28)
		$^8A_2$			3.07 (2.35)
		$^6B_2$			3.66 (2.93)
	η^1-MnS_2^-	$^7A_1$ ($^7\Sigma^+$)			2.22

[a]Frequencies are arranged in the order of SMnS bending, Mn−S symmetric stretching, and Mn−S asymmetric stretching modes for the linear $SMnS^{0/-}$ isomer; asymmetric Mn−S stretching, Mn−S symmetric stretching, and S−S stretching mode for the η^2-$MnS_2^{0/-}$ isomers; and Mn−S stretching, SMnS bending, and S−S stretching mode for η^1-$MnS_2^{-/0}$. [b]CCSD(T) single-point energies as calculated at the B3LYP geometries. [c]Values in parentheses are ARE as compared to the $^7A_1$ of the η^2-MnS_2^- isomer.

DOI: 10.1021/acs.jpca.5b02896
J. Phys. Chem. A XXXX, XXX, XXX−XXX

Table 2. Leading Configurations, Geometric Parameters, and Adiabatic and Vertical Relative Energies (ARE and VRE) of the Low-Lying States of the $MnS_2^{-/0}$ Clusters As Computed with NEVPT2[a]

cluster	state	leading configuration	weight (%)	Mn−S (Å), SMnS (deg), S−S (Å)	ARE[a] (eV)	VRE[a] (eV)	expt (eV) ADE	expt (eV) VDE
$SMnS^-$	$^5A_2$ ($^5\Pi_g$)	$12a_1^2 13a_1^1 14a_1^1 4b_1^2 5b_1^1 8b_2^2 9b_2^2 10b_2^1 2a_2^2 3a_2^0$	65	2.126, 180.00	0.00	0.00		
	$^5B_2$ ($^5\Pi_g$)	$12a_1^2 13a_1^1 14a_1^1 4b_1^2 5b_1^1 8b_2^2 9b_2^2 10b_2^0 2a_2^2 3a_2^1$	62	2.126, 154.50	0.09			
	$^5A_1$	$12a_1^1 13a_1^1 14a_1^1 4b_1^2 5b_1^1 8b_2^2 9b_2^2 10b_2^1 2a_2^2 3a_2^1$	53			1.43		
	$^5B_1$	$12a_1^2 13a_1^1 14a_1^1 4b_1^1 5b_1^1 8b_2^2 9b_2^2 10b_2^1 2a_2^2 3a_2^1$	71			1.39		
	$^7A_1$	$12a_1^1 13a_1^1 14a_1^1 4b_1^2 5b_1^1 8b_2^2 9b_2^2 10b_2^1 2a_2^2 3a_2^1$	88			1.06		
	$^7A_2$	$12a_1^2 13a_1^1 14a_1^1 4b_1^2 5b_1^1 8b_2^2 9b_2^2 10b_2^1 2a_2^1 3a_2^1$	90			1.21		
	$^7B_1$	$12a_1^2 13a_1^1 14a_1^1 4b_1^1 5b_1^1 8b_2^2 9b_2^2 10b_2^1 2a_2^2 3a_2^1$	88			1.03		
	$^7B_2$	$12a_1^2 13a_1^1 14a_1^1 4b_1^2 5b_1^1 8b_2^2 9b_2^1 10b_2^1 2a_2^2 3a_2^1$	88			1.28		
SMnS	$^4B_1$ ($^4\Sigma_g^-$)	$12a_1^2 13a_1^1 14a_1^1 4b_1^2 5b_1^1 8b_2^2 9b_2^2 10b_2^0 2a_2^2 3a_2^0$	46	2.073, 140.43	2.67	2.73	2.94	3.04
	$^4B_2$	$12a_1^1 13a_1^1 14a_1^1 4b_1^2 5b_1^1 8b_2^2 9b_2^2 10b_2^0 2a_2^2 3a_2^1$	33	2.217, 180.00	3.32	3.38		
	$^4A_2$	$12a_1^1 13a_1^1 14a_1^1 4b_1^2 5b_1^1 8b_2^2 9b_2^2 10b_2^1 2a_2^2 3a_2^0$	11	2.218, 180.00	3.34	3.46		
	$^6B_2$	$12a_1^2 13a_1^1 14a_1^1 4b_1^1 5b_1^1 8b_2^2 9b_2^2 10b_2^1 2a_2^2 3a_2^0$	36	2.231, 180.00	3.44	3.58		
	$^6B_1$	$12a_1^2 13a_1^1 14a_1^1 4b_1^2 5b_1^1 8b_2^1 9b_2^2 10b_2^1 2a_2^1 3a_2^1$	19	2.242, 180.00	3.51	3.68		
	$^6A_1$	$12a_1^2 13a_1^1 14a_1^1 4b_1^2 5b_1^1 8b_2^2 9b_2^2 10b_2^1 2a_2^1 3a_2^0$	41	2.268, 180.00	3.58	3.83		
η^2-MnS_2^-	$^7A_1$	$13a_1^1 14a_1^1 15a_1^1 5b_1^1 9b_2^1 2a_2^2 3a_2^1$	96	2.341, 55.94	0.96 (0.00)	(0.00)		
	$^5A_1$	$13a_1^2 14a_1^1 15a_1^0 5b_1^1 9b_2^1 2a_2^2 3a_2^1$	34	2.323, 57.10	1.77 (0.81)			
η^2-MnS_2	$^6A_1$	$13a_1^1 14a_1^1 15a_1^0 5b_1^1 9b_2^1 2a_2^2 3a_2^1$	93	2.209, 62.16	2.89 (1.93)	(2.27)	1.3−2.8	
	$^6A_2$	$13a_1^1 14a_1^1 15a_1^1 5b_1^1 9b_2^1 2a_2^2 3a_2^0$	34	2.463, 48.77	3.03 (2.07)	(2.32)		
	$^8A_2$	$13a_1^1 14a_1^1 15a_1^1 5b_1^1 9b_2^1 2a_2^1 3a_2^1$	96	2.480, 48.39	3.04 (2.08)	(2.37)		
	$^6B_2$	$13a_1^1 14a_1^1 15a_1^1 5b_1^1 9b_2^0 2a_2^2 3a_2^1$	56	2.381, 51.05	3.44 (2.48)	(2.62)		
η^1-MnS_2^-	$^7A_1$ ($^7\Sigma^+$)	$15a_1^1 16a_1^1 17a_1^1 7b_1^1 7b_2^1 1a_2^1$	98	2.141, 180, 2.089	2.58			
η^1-MnS_2	$^6B_1$ ($^6\Pi$)	$15a_1^1 16a_1^1 17a_1^1 7b_1^0 7b_2^1 1a_2^1$	39	2.231, 180, 1.991	4.34			

[a]For one-electron detachment processes ARE and VRE denote the adiabatic and vertical detachment energies. Numbers in parentheses are ARE and VRE as compared to the $^7A_1$ of the η^2-MnS_2^- isomer.

bonds or bending the SMnS angle. The profiles for the bending mode allow to check the stability of the η^2-$MnS_2^{-/0}$ isomers in respect with their lower positioned linear $SMnS^{-/0}$ counterparts. The stretching mode profiles are important for the purpose of performing harmonic vibrational frequency analyses. These frequencies and equilibrium geometries were subsequently employed for Franck−Condon factor simulations. All NEVPT2 data were obtained with the DALTON suite of programs.[41,42]

RESULTS AND DISCUSSION

Stability of Different Isomers of $MnS_2^{-/0}$. The relative stabilities of the various isomers, namely $SMnS^{-/0}$, η^2-$MnS_2^{-/0}$, and η^1-$MnS_2^{-/0}$ were obtained by the B3LYP, CCSD(T), and NEVPT2 methods. The B3LYP and CCSD(T) results are collected in Table 1, while NEVPT2 results are shown in Table 2. For the anionic isomers, at all three levels of computation the most stable electronic state is identified as $^5\Pi_g$ ($^5A_2$, $^5B_2$) of the linear $SMnS^-$ cluster. Other quintets states and all calculated septets, as included in Table 2, are positioned more than 1 eV higher. Most likely they are not involved in the anion photoelectron spectroscopy, so they were not further investigated at the CCSD(T) and B3LYP levels or concerning their nature. At the NEVPT2 level the $^5\Pi_g$ is split into the more stable quasi linear $^5A_2$ state and the less stable bent $^5B_2$ state with a SMnS angle of 154.50°. Apparently, the Renner−Teller effect causes the largest distortion for the latter state. The effect on the energy of such states has been known to be quite small,[19] and this appears to be the case here where the splitting between the two components of $^5\Pi_g$ amounts to just 0.09 eV. Also the potential energy curve for the S−Mn−S bending mode is quite flat (vide infra). Therefore, as an acceptable approximation, the ground state of the most stable $SMnS^-$ isomer can be labeled as $^5\Pi_g$. The $^7A_1$ of the η^2-MnS_2^- and the $^7\Sigma^+$ ($^7A_1$) of the η^1-MnS_2^- are, respectively, 0.96 and 2.58 eV less stable than this anionic ground state as calculated by NEVPT2. The same relative stabilities were found with the B3LYP and CCSD(T) methods. In particular, these two septet states are placed above the anionic ground state at 1.00 and 2.20 eV by B3LYP, and at 0.73 and 2.22 eV by CCSD(T). All these results manifestly allow to deduce that the anionic ground state is the $^5\Pi_g$ ($^5A_2$, $^5B_2$) state of the $SMnS^-$ isomer, which consequently is the initial state responsible for the high intensity band of the experimental photoelectron spectrum.

For the neutral cluster a comparable stability for the $^4B_1$ ($^4\Sigma_g^-$) of the linear SMnS and $^6A_1$ of the η^2-MnS_2 isomers was found. At the NEVPT2 level, the relative energies of these states, as compared to the anionic ground state, are 2.67 and 2.89 eV, respectively, meaning that the quartet is only 0.22 eV more stable than the sextet. However, at the single-reference B3LYP and CCSD(T) levels the relative energy order is inverted as compared to NEVPT2, with a smaller energy difference of around 0.16 eV. It should be noted that the $^4B_1$ ($^4\Sigma_g^-$) possesses a pronounced multireference wave function with a weight for the leading configuration of 46%. Therefore, the single-reference B3LYP and CCSD(T) methods are not flexible enough to describe adequately the quartet and thereby underestimate the stability of this state. We are consequently inclined to accept that under these circumstances, NEVPT2 is more reliable than both B3LYP and CCSD(T) and, therefore, propose the $^4B_1$ ($^4\Sigma_g^-$) state as the ground state of the neutral cluster.

DOI: 10.1021/acs.jpca.5b02896
J. Phys. Chem. A XXXX, XXX, XXX−XXX

Electronic Structures of $MnS_2^{-/0}$. The electronic structures of the $MnS_2^{-/0}$ clusters are most easily identified by analyzing the corresponding CASSCF wave functions. For the linear $SMnS^{-/0}$ isomers, CASSCF molecular orbital plots and electron occupation numbers for the anionic $^5\Pi_g$ ($^5A_2$) ground state are shown in Figure 2. In this figure all

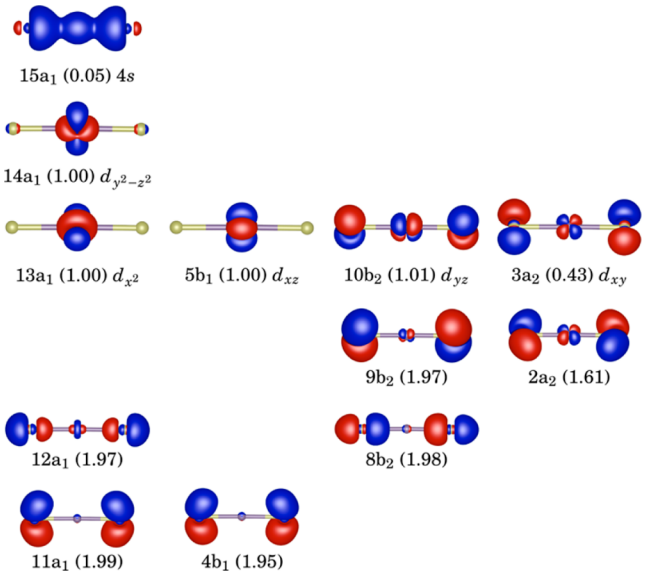

Figure 2. Pseudonatural CASSCF orbitals and the corresponding electron occupation numbers for the $^5A_2$ ($^5\Pi_g$) state of the $SMnS^-$ cluster.

predominantly 3p orbitals of S, namely $11a_1$, $12a_1$, $4b_1$, $8b_2$, $9b_2$, and $2a_2$, are doubly occupied. The metal $3d_{x^2}$ ($13a_1$), $3d_{y^2-z^2}$ ($14a_1$), $3d_{xz}$ ($5b_1$), and $3d_{yz}$ ($10b_2$) are singly occupied, while the $3d_{xy}$ ($3a_2$) and 4s ($15a_1$) are unoccupied. This occupation of the valence orbitals allows to schematically summarize the electronic structure of the anionic ground state formally as $(S^{2-})(Mn^{3+})(S^{2-})$. By transferring an electron from $3d_{yz}$ ($10b_2$) to $3d_{xy}$ ($3a_2$), the $^5B_2$ state can be obtained. It should be noted that these are d_π orbitals and therefore $^5A_2$ and $^5B_2$ are two components of a $^5\Pi_g$ state. Otherwise, the detachment of one electron from the $3d_\pi$ ($10b_2$) orbital of $^5\Pi_g$ anionic ground state results in the $^4B_1$ ($^4\Sigma_g^-$) neutral ground state.

The CASSCF molecular orbitals of the $^7A_1$, the lowest energy state of η^2-MnS_2^-, are shown in Figure 3. Of the six predominantly 3p orbitals of S, five are doubly occupied ($11a_1$, $12a_1$, $4b_1$, $8b_2$, and $2a_2$) and one is unoccupied ($10b_2$ (σ^*)). All 3d and 4s orbitals of Mn, labeled as $3d_{x^2}$ ($13a_1$), $3d_{y^2-z^2}$ ($14a_1$), 4s,4p ($15a_1$), $3d_{xz}$ ($5b_1$), $3d_{yz}$ ($9b_2$), and $3d_{xy}$ ($3a_2$) are singly occupied. This corresponds to the following formal charge distribution for this state: $(Mn^+)(S_2^{2-})$. Due to the lower oxidation state of the manganese cation, the 4s,4p orbital is occupied by one electron in this state. The lowest energy $^6A_1$ state of η^2-MnS_2 can be obtained by detaching an electron from the 4s,4p ($15a_1$) orbital of the $^7A_1$ state of the anionic cluster.

Figure 4 depicts the CASSCF molecular orbitals of the $^7\Sigma^+$ ($^7A_1$) for the η^1-MnS_2^- isomer. Similar to the $^7A_1$ of the η^2-MnS_2^- isomer, all 3d ($15a_1$, $16a_1$, $7b_1$, $7b_2$, and $1a_2$) and 4s,4p ($17a_1$) orbitals of Mn of $^7\Sigma^+$ ($^7A_1$) are singly occupied. Concerning the six predominantly 3p orbitals of S, only the σ^* ($18a_1$) is unoccupied while the remaining orbitals ($14a_1$, $5b_1$, $6b_1$, $5b_2$, and $6b_2$) are doubly occupied. By detaching the

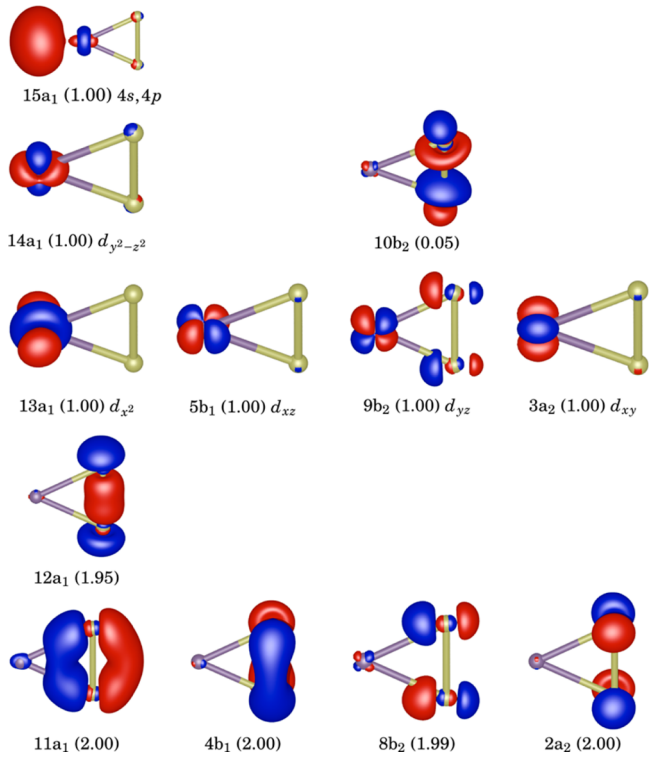

Figure 3. Pseudonatural CASSCF orbitals and the corresponding electron occupation numbers of the $^7A_1$ state of the η^2-MnS_2^- cluster.

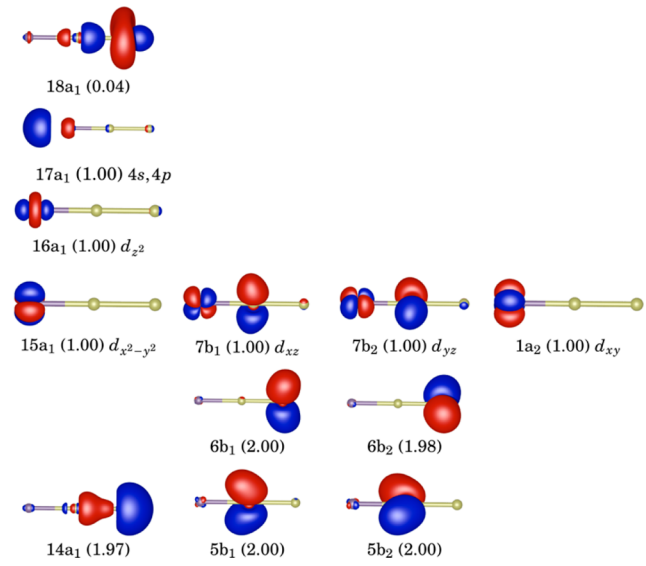

Figure 4. Pseudonatural CASSCF orbitals and the corresponding electron occupation numbers of the $^7A_1$ ($^7\Sigma^+$) state of the η^1-MnS_2^- cluster.

electron from the $7b_1$ (d_π) orbital of the $^7\Sigma^+$ state, the lowest energy $^6\Pi$ ($^6B_1$) state of the neutral η^1-MnS_2 isomer is obtained.

From the electronic structures and corresponding weights of the leading configurations of the low-lying electronic states of $MnS_2^{-/0}$ as included in Table 2, it is possible to deduce that the multireference character is for many relevant states quite pronounced. In particular, for the linear SMnS cluster, all states in the region of relative energies from 2.67 to 3.58 eV show a reference weight of less than 46%. The ground state $^5\Pi_g$ of the

DOI: 10.1021/acs.jpca.5b02896
J. Phys. Chem. A XXXX, XXX, XXX−XXX

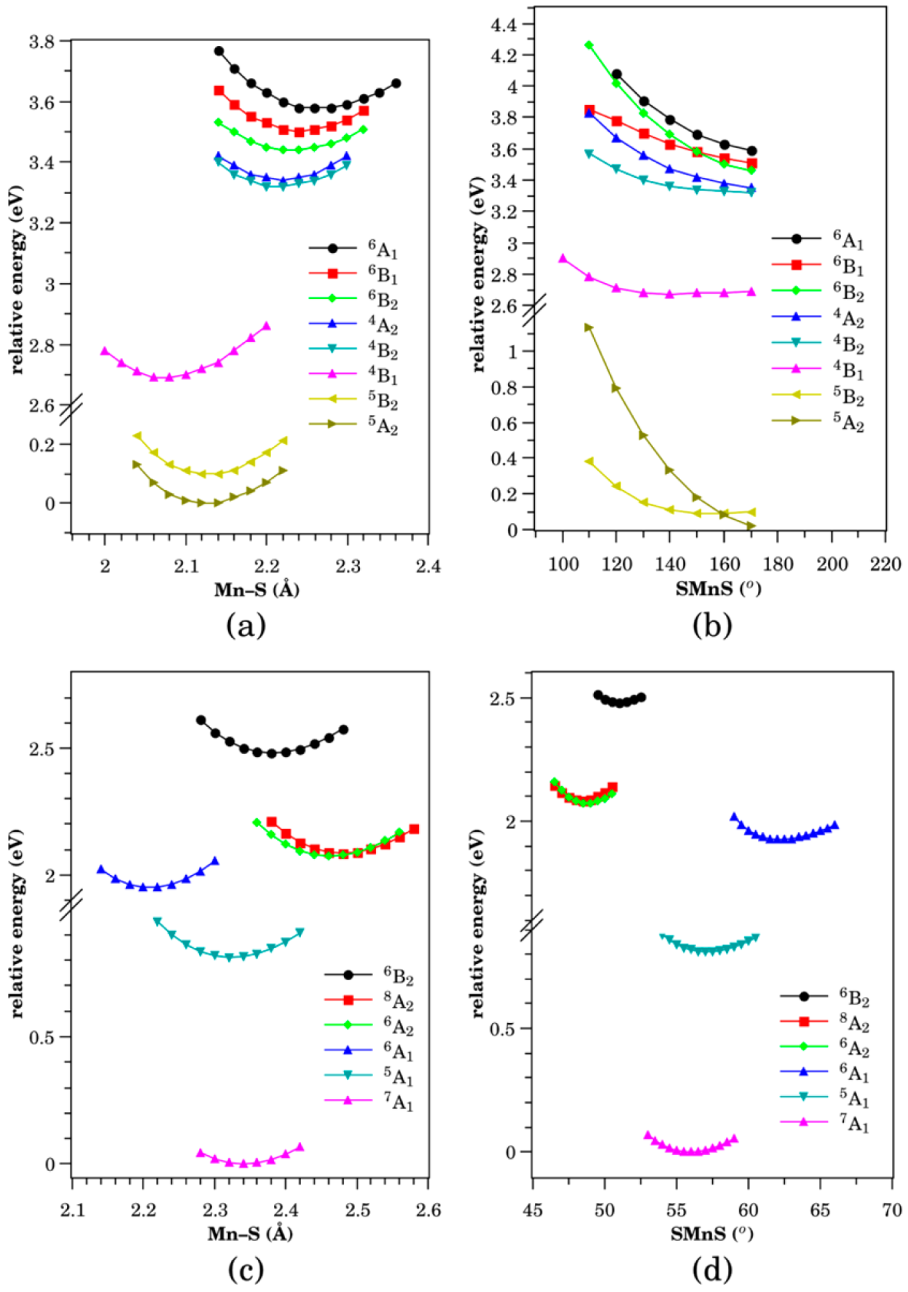

Figure 5. Potential energy profiles for the symmetric Mn−S stretch and SMnS bending for $SMnS^{-/0}$ (a and b, respectively), and for η^2-$MnS_2^{-/0}$ (c and d, respectively) as obtained at the NEVPT2 level.

neutral $SMnS^-$ isomer possesses a weight for the leading configuration of around 65%. Other states in this kind are $^5A_1$ (34%), $^6A_2$ (34%), and $^6B_2$ (56%) of the η^2-$MnS_2^{-/0}$, and $^6\Pi$ ($^6B_1$) (39%) of η^1-MnS_2. Due to this manifest multireference nature of many of the low-lying electronic states, a computational investigation of the electronic structures of $MnS_2^{-/0}$ requires an appropriate wave function method, such as NEVPT2. The electronic structures of the $MnS_2^{-/0}$ clusters are essential for an unambiguous interpretation of the anion photoelectron spectrum, in the sense that they are indispensable for identifying the one-electron detachment processes.

Potential Energy Profiles of the Low-Lying States of $MnS_2^{-/0}$ Clusters. Starting from the B3LYP geometries, the potential energy profiles for the symmetric stretching of the two Mn−S bonds and the bending of SMnS angle were constructed for the low-lying states of the linear $SMnS^{-/0}$ and η^2-$MnS_2^{-/0}$ clusters at the NEVPT2 level. For the $SMnS^{-/0}$ isomers, the resulting potential energy profiles are displayed in Figure 5a and b, respectively. The former potential energy profile affords a bond distance of 2.126 Å for the $^5\Pi_g$ ground state of the anionic linear isomer. On the other hand, for the bending of SMnS angle, there is a splitting of the $^5\Pi_g$ due to a Renner−Teller distortion. In particular, the equilibrium geometry of the $^5A_2$ component almost retains a linear structure, while the $^5B_2$ component has a much smaller angle with an equilibrium value of 154.50°. However, such distortions from the linear structures have been known to be quite small in energy, as previously calculated for the $^2\Delta_g$ and $^3\Delta_g$ states of the FeO_2^- cluster.[19] Clearly, this is also the case for the potential energy curves for the states included in Figure 5b. Most

DOI: 10.1021/acs.jpca.5b02896
J. Phys. Chem. A XXXX, XXX, XXX−XXX

interesting, the $^5B_2$ possesses a flat potential energy profile, especially when the SMnS bond angle changes from 140° to 180°, with a minimum at 154.50°. However, the energy of this equilibrium geometry is only 70 cm^{-1} lower than the linear structure. Such a small distortion energy is even much lower than the zero point energy of 406 cm^{-1} of the $^5B_2$ as calculated at the B3LYP level. Consequently, the two S atoms will vibrate around the linear structure, which implies that under all experimental conditions, a linear structure would be detected. Similar to $^5B_2$, $^4B_1$ also shows a very flat potential energy profile for the SMnS bending mode in the region from 130° to 180°. The energy difference between the minimum at 140.43° and the linear structure is 114 cm^{-1}, also meaning that experimentally a linear structure will be observed for this state. For all practical reasons, the $^5B_2$ and $^4B_1$ can be approximated to possess linear structures. In the remainder of this paper they are therefore referenced to as $^5\Pi_g$ and $^4\Sigma_g^-$, respectively.

Potential energy profiles for the η^2-$MnS_2^{-/0}$ isomers, as constructed at the NEVPT2 level are shown in Figures 5c and d. Previous DFT results showed that there is a continuous potential energy decrease from the η^2-MnS_2 cluster to the linear SMnS cluster.[16] However, our potential energy curves for the bending of the SMnS angle in Figure 5d, clearly show minima at 55.94° for the $^7A_1$ state of the anionic η^2-MnS_2^- isomer and at 62.16° for $^6A_1$ of neutral η^2-MnS_2 isomer. Moreover, for the symmetric stretching of the Mn−S bonds, a minimum is located at 2.341 Å for $^7A_1$ and of 2.209 Å for $^6A_1$. These minima are also confirmed by B3LYP geometry optimizations and harmonic vibrational frequencies. Therefore, both the B3LYP and NEVPT2 results imply that the lowest energy states of η^2-$MnS_2^{-/0}$ isomers, namely the $^7A_1$ and $^6A_1$, exist as local minima on potential energy surface. By increasing the SMnS bond angles of Figure 5d further to values of 120°, it was found at the NEVPT2 level that these states have both deep potential energy wells of more than 1 eV (not depicted). This outcome is in sharp contrast to the previous DFT study that was unable to identify stable η^2-MnS_2 structures.[16]

Assignment of Photoelectron Spectrum of MnS_2^-. The photoelectron spectrum of MnS_2^- was measured with a photon energy of 355 nm or 3.49 eV. As presented in Figure 6, this spectrum shows two features.[10] The first one at binding energies ranging from 1.3 to 2.8 eV is very broad and has a very low intensity. The second band has an unresolved vibrational progression due to the low resolution and exhibits a sharp peak at a binding energy of 2.94 eV. Due to the low intensity of the first band, as compared to the second band, the experimental photoelectron spectrum of MnS_2^- was explained by a coexistence of two structural isomers. The first low intensity band was attributed to a flexible η^2-MnS_2 isomer, while the second band was ascribed to a rigid linear $SMnS^{-/0}$ structure. Assignment of the latter band was afterward confirmed by DFT calculations with an electron affinity of 2.80 eV, which is in good agreement with the peak position of the second band.[16] Rather surprisingly, as the first feature was thought to originate from the η^2-$MnS_2^{-/0}$ clusters, the geometric and electronic structures of these clusters have not been reported yet at any level of computation.

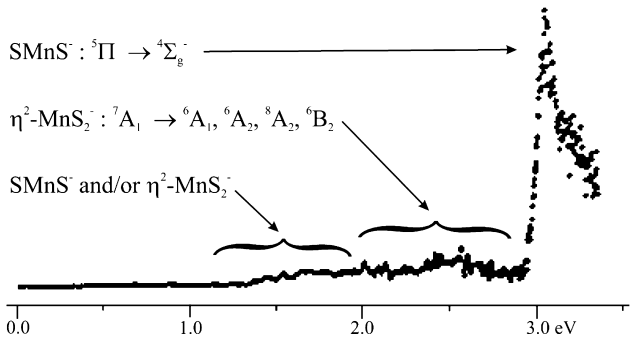

Figure 6. Experimental photoelectron spectrum of MnS_2^- as reported in ref 10 and assignments as derived from the computational data of the present contribution.

Because the $^5\Pi_g$ state of $SMnS^-$ is computed as the ground state of the anionic cluster, this state is used as the initial state for electron detachment processes in the photoelectron spectrum of MnS_2^-. From the above discussion of the electronic structures of the various electronic states, the transition from the anionic ground state $^5\Pi_g$ to the neutral ground state $^4\Sigma_g^-$ is accomplished by removing an electron from the $10b_2$ (d_π) orbital. The adiabatic detachment energy of this transition is 3.13, 3.07, and 2.67 eV as computed with B3LYP, CCSD(T), and NEVPT2, respectively. These values are in reasonable agreement with the peak position of 2.94 eV for the second band in the spectrum. The vertical detachment energy for this transition at the NEVPT2 level is 2.73 eV and therefore also corresponds well with the experimental proposed value of 3.04 eV. In general, the calculated results show that the second band in the photoelectron spectrum of MnS_2^- is the result of the $^5\Pi_g \rightarrow {}^4\Sigma_g^-$ transition within $SMnS^{-/0}$ clusters. This assignment of the second band is in agreement with the previous DFT results.[16] However, the nature of the responsible electronic states was not specified.

In order to make sure that the second band in the spectrum is the result of the $^5\Pi_g \rightarrow {}^4\Sigma_g^-$ transition between the $SMnS^{-/0}$ isomers, a Franck−Condon factor simulation based on the NEVPT2 potential energy profiles of Figure 5a−d, is performed. As already mentioned above, the potential energy curve for the bending mode of the $^4\Sigma_g^-$ is very flat for SMnS bond angles between 130° and 180°. Therefore, the frequencies associated with this vibrational mode will be quite small and consequently will not contribute to the shape of the band. On the other hand, the harmonic vibrational analyses of the potential energy profiles of the symmetric stretching of the linear $SMnS^{-/0}$ clusters, render frequencies of 389 cm^{-1} for $^5\Pi_g$ and 382 cm^{-1} for $^4\Sigma_g^-$. The Franck−Condon factor simulation for the $^5\Pi_g \rightarrow {}^4\Sigma_g^-$ transition, as depicted in Figure 7, shows a vibrational progression of four peaks, of which the first peak has the highest intensity. It should be noted that the silhouette of the second band in the photoelectron spectrum corresponds quite will with these results.[10] Indeed, it starts with a sharp peak at 3.04 eV with a gradual decline toward higher binding energies. Overall, we can conclude that the second band in the spectrum is the result of the $^5\Pi_g \rightarrow {}^4\Sigma_g^-$ ionization between the linear $SMnS^{-/0}$ clusters.

Due to its much lower intensity than the second band, the first band with binding energy at 1.30−2.80 eV in the spectrum, should be attributed to the less stable η^2-MnS_2^- isomer instead of the most stable linear $SMnS^{-/0}$ isomer. Our NEVPT2 results in Table 2 show that the lowest energy $^7A_1$ state of cyclic anionic cluster is 0.96 eV less stable than the $^5A_2$ ground state of $SMnS^-$ cluster and 1.62 eV more stable than the $^7\Sigma^+$ ($^7A_1$) of η^1-MnS_2^-. Therefore, the $^7A_1$ of the η^2-MnS_2^- cluster is used as the initial state to explain the first band. Of course, the very low

DOI: 10.1021/acs.jpca.5b02896
J. Phys. Chem. A XXXX, XXX, XXX−XXX

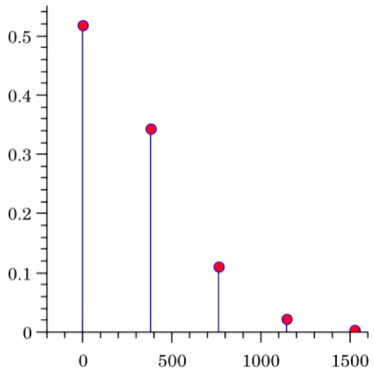

Figure 7. Franck−Condon factor simulation for the $^5\Pi_g \rightarrow {}^4\Sigma_g^-$ transition between the ground states of the $SMnS^{-/0}$ clusters at the NEVPT2 level.

intensity of the first band is then explained by the most likely low population of the $^7A_1$ state of the η^2-MnS_2^- cluster in the experiment. The first band is also very broad which indicates that it may exist of a few low-energy electron detachment processes for this isomer. This is indeed the case here since one-electron detachments from the $^7A_1$ result in the $^6A_1$, $^6A_2$, $^8A_2$, and $^6B_2$ states. The corresponding adiabatic detachment energies are 1.93, 2.07, 2.08, and 2.48 eV, while the vertical detachment energies are 2.27, 2.32, 2.37, and 2.62 eV. For these ionization processes, detachments of an electron from the 3d and 4s orbitals of Mn give rise to the three sextets, while an ionization from the predominantly $2a_2$ (π^*) orbital of the S_2 ligand results in the octet state. The lower ionization energy of 1.93 eV between the lowest states of the anionic and neutral cyclic isomers ($^7A_1$ to $^6A_1$), when compared with the linear SMnS isomer, is the outcome of the higher oxidation of the manganese center in the latter isomers. Indeed, as a consequence, in the anionic $^5\Pi_g$ ground state the 4s,4p orbital is not occupied, resulting in a higher adiabatic detachment energy of 2.67 eV. In conclusion, the electron detachments processes from the $^7A_1$ of the η^2-MnS_2^- isomers explain the low intensity feature in the photoelectron spectrum starting from 1.90 eV to the beginning of the high intensity second band.

From the discussion above it is clear that there is still no ionization identified with detachment energies of around 1.30 eV, which is the starting point of the first feature in the experimental spectrum. Because of the extremely low intensity of the spectrum in this region, it may be attributed to several ionization processes. As will become clear we cannot identify with certainty which of these transitions are indeed at the origin of the experimental signal. Just as an example, a first possible assignment corresponds to a one-electron detachment from the first electronic excited $^5A_1$ state of the η^2-MnS_2^- isomer. Indeed, the removal of an electron from the $13a_1$ (d_{x^2}) orbital of this state results in the neutral $^6A_1$ with an adiabatic detachment energy of 1.12 eV, which agrees with the threshold of the first band of 1.30 eV. As a second possibility, a two-electron transition process from an excited state of the $SMnS^-$ isomer might also be at the origin of the low-energy part of the spectrum. It is therefore safe to conclude that due to the fact that the experimental intensity of this low-energy feature is extremely low, many electronic transitions can explain the first band in the spectrum. Also, this low intensity prevented to measure the exact starting point and to recognize possible contributions of different electron detachment processes in the region from 1.30 to 2.80 eV. Higher resolution photoelectron spectroscopy for the MnS_2^- clusters is obviously needed to reach a more detailed picture about the structural and electronic properties, and therefore constitutes a challenge for future experimental and theoretical studies.

CONCLUSIONS

The geometric and electronic structures of three isomers of $MnS_2^{-/0}$ clusters, namely the $SMnS^{-/0}$, η^2-$MnS_2^{-/0}$, and η^1-$MnS_2^{-/0}$, have been investigated by B3LYP, CCSD(T), and NEVPT2. The results show that for the neutral cluster, the $^4\Sigma_g^-$ state of SMnS and the $^6A_1$ state of η^2-MnS_2 have almost the same stability. On the other hand, the ground state of anionic cluster is distinctly calculated as the $^5\Pi_g$ of the linear $SMnS^-$ isomer. Consequently, the highest intensity band at a binding energy of 2.94 eV in the experimental photoelectron spectrum of MnS_2^- is attributed to the one-electron detachment from the $^5\Pi_g$ to the $^4\Sigma_g^-$ state within the linear SMnS isomer. The adiabatic detachment energies for this experimental feature, as calculated by DFT, CCSD(T), and NEVPT2 are respectively 3.12, 3.07, and 2.67 eV which match the experimental value of 2.94 eV very well. A Franck−Condon factor simulation for the $^5\Pi_g \rightarrow {}^4\Sigma_g^-$ transition also confirms the broad shape of this band. The very low intensity feature at binding energies between 1.30 and 2.80 eV in the experimental spectrum, is partly ascribed to the electron detachments from the less stable η^2-$MnS_2^{-/0}$ isomer. The $^7A_1$ of η^2-MnS_2^- is computed to 1.00, 0.73, and 0.96 eV less stable than the $^5A_2$ ground state of the $SMnS^-$ isomer by B3LYP, CCSD(T), and NEVPT2 methods, so that this state is possibly the initial state for the electron detachments at the high-energy side of the low-intensity first band. The NEVPT2 results afford adiabatic detachment energies of 1.93, 2.07, 2.08, and 2.48 eV for transitions from $^7A_1$ to $^6A_1$, $^6A_2$, $^8A_2$, and $^6B_2$, respectively. Vertical detachment energies for these transitions are evaluated as 2.27, 2.32, 2.37, and 2.62 eV. These adiabatic and vertical detachment energies are in the region from 1.90 to 2.8 eV of the first band. Unfortunately, there is no one-electron detachment processes from the $^7A_1$ of η^2-MnS_2^- which corresponds to the starting point of the first band at binding energies at 1.30 eV. However, several transitions from excited anionic states of either $SMnS^-$ or η^2-MnS2$^-$ isomers can possible be at the origin of the lowest energy part of the spectrum. Because of the experimental low intensity of this part of the spectrum no final conclusion could be reached. On the whole, the presented computational results allow to conclude that the entire photoelectron spectrum of the MnS_2^- cluster must be attributed to an experimental coexistence of the $SMnS^-$ and cyclic-MnS_2^- isomers.

AUTHOR INFORMATION

Corresponding Author

*E-mail: marc.hendrickx@chem.kuleuven.be. Tel.: +32 16 32 73 62.

Notes

The authors declare no competing financial interest.

REFERENCES

(1) Stiefel Edward, I. Transition Metal Sulfur Chemistry: Biological and Industrial Significance and Key Trends. In *Transition Metal Sulfur Chemistry*; American Chemical Society, 1996; Vol. *653*; pp 2−38.

(2) Harris, S.; Chianelli, R. R. Catalysis by Transition Metal Sulfides: The Relation Between Calculated Electronic Trends and HDS Activity. *J. Catal.* **1984**, *86*, 400−412.

DOI: 10.1021/acs.jpca.5b02896
J. Phys. Chem. A XXXX, XXX, XXX−XXX

(3) Liang, B.; Andrews, L. Infrared Spectra and Density Functional Theory Calculations of Group 4 Transition Metal Sulfides. *J. Phys. Chem. A* **2002**, *106*, 6295−6301.
(4) Liang, B.; Andrews, L. Infrared Spectra and Density Functional Theory Calculations of Group 6 Transition Metal Sulfides in Solid Argon. *J. Phys. Chem. A* **2002**, *106*, 6945−6951.
(5) Liang, B.; Andrews, L. Infrared Spectra and Density Functional Theory Calculations of Group V Transition Metal Sulfides. *J. Phys. Chem. A* **2002**, *106*, 3738−3743.
(6) Liang, B.; Wang, X.; Andrews, L. Infrared Spectra and Density Functional Theory Calculations of Group 10 Transition Metal Sulfide Molecules and Complexes. *J. Phys. Chem. A* **2009**, *113*, 3336−3343.
(7) Liang, B.; Wang, X.; Andrews, L. Infrared Spectra and Density Functional Theory Calculations of Group 8 Transition Metal Sulfide Molecules. *J. Phys. Chem. A* **2009**, *113*, 5375−5384.
(8) Zhai, H.-J.; Kiran, B.; Wang, L.-S. Electronic and Structural Evolution of Monoiron Sulfur Clusters, FeS_n^- and FeS_n (n = 1−6), from Anion Photoelectron Spectroscopy. *J. Phys. Chem. A* **2003**, *107*, 2821−2828.
(9) Zhang, N.; Hayase, T.; Kawamata, H.; Nakao, K.; Nakajima, A.; Kaya, K. Photoelectron Spectroscopy of Iron-Sulfur Cluster Anions. *J. Chem. Phys.* **1996**, *104*, 3413−3419.
(10) Zhang, N.; Kawamata, H.; Nakajima, A.; Kaya, K. Photoelectron Spectroscopy of Manganese-Sulfur Cluster Anions. *J. Chem. Phys.* **1996**, *104*, 36−41.
(11) Clima, S.; Hendrickx, M. F. A. Interpretation of the Photoelectron Spectra of FeS_2^- by a Multiconfiguration Computational Approach. *J. Phys. Chem. A* **2007**, *111*, 10988−10992.
(12) Clima, S.; Hendrickx, M. F. A. Photoelectron Spectra of FeS^- Explained by a CASPT2 Ab Initio Study. *Chem. Phys. Lett.* **2007**, *436*, 341−345.
(13) Tran, V. T.; Hendrickx, M. F. A. Assignment of the Photoelectron Spectra of FeS_3^- by Density Functional Theory, CASPT2, and RCCSD(T) Calculations. *J. Phys. Chem. A* **2011**, *115*, 13956−13964.
(14) Tran, V. T.; Hendrickx, M. F. A. Molecular Structures for $FeS_4^{-/0}$ As Determined from an ab Initio Study of the Anion Photoelectron Spectra. *J. Phys. Chem. A* **2013**, *117*, 3227−3234.
(15) Hübner, O.; Sauer, J. The electronic states of $Fe_2S_2^{-/0/+/2+}$. *J. Chem. Phys.* **2002**, *116*, 617−628.
(16) Dance, I. G.; Fisher, K. J. Density Functional Calculations of Electronic Structure, Geometric Structure and Stability for Molecular Manganese Sulfide Clusters. *J. Chem. Soc., Dalton Trans.* **1997**, 2563−2576.
(17) Tran, V. T.; Hendrickx, M. F. A. Description of the Geometric and Electronic Structures Responsible for the Photoelectron Spectrum of FeO_4^-. *J. Chem. Phys.* **2011**, *135*, 094505.
(18) Hendrickx, M. F. A.; Tran, V. T. Elucidating the Electronic Structures of the Ground States of the $VO_2^{-/0}$ Clusters: Synergism between Computation and Experiment. *J. Chem. Theory Comput.* **2014**, *10*, 4037−4044.
(19) Hendrickx, M. F. A.; Tran, V. T. On the Electronic and Geometric Structures of $FeO_2^{-/0}$ and the Assignment of the Anion Photoelectron Spectrum. *J. Chem. Theory Comput.* **2012**, *8*, 3089−3096.
(20) Angeli, C.; Cimiraglia, R.; Evangelisti, S.; Leininger, T.; Malrieu, J.-P. Introduction of n-Electron Valence States for Multireference Perturbation Theory. *J. Chem. Phys.* **2001**, *114*, 10252−10264.
(21) Angeli, C.; Cimiraglia, R.; Malrieu, J.-P. N-Electron Valence State Perturbation Theory: a Fast Implementation of the Strongly Contracted Variant. *Chem. Phys. Lett.* **2001**, *350*, 297−305.
(22) Angeli, C.; Cimiraglia, R.; Malrieu, J.-P. N-Electron Valence State Perturbation Theory: A Spinless Formulation and an Efficient Implementation of the Strongly Contracted and of the Partially Contracted Variants. *J. Chem. Phys.* **2002**, *117*, 9138−9153.
(23) Schapiro, I.; Sivalingam, K.; Neese, F. Assessment of n-Electron Valence State Perturbation Theory for Vertical Excitation Energies. *J. Chem. Theory Comput.* **2013**, *9*, 3567−3580.
(24) Angeli, C.; Cimiraglia, R. A Multireference Perturbation Theory Study on the Fe_2 Molecule: in Quest of the Ground State. *Mol. Phys.* **2011**, *109*, 1503−1509.
(25) Atanasov, M.; Comba, P.; Helmle, S.; Müller, D.; Neese, F. Zero-Field Splitting in a Series of Structurally Related Mononuclear Ni^{II}-Bispidine Complexes. *Inorg. Chem.* **2012**, *51*, 12324−12335.
(26) Atanasov, M.; Zadrozny, J. M.; Long, J. R.; Neese, F. A Theoretical Analysis of Chemical Bonding, Vibronic Coupling, and Magnetic Anisotropy in Linear Iron(II) Complexes with Single-Molecule Magnet Behavior. *Chem. Sci.* **2013**, *4*, 139−156.
(27) Camacho, C.; Witek, H. A.; Cimiraglia, R. The Low-Lying States of the Scandium Dimer. *J. Chem. Phys.* **2010**, *132*, 244306.
(28) Domingo, A.; Carvajal, M.; de Graaf, C.; Sivalingam, K.; Neese, F.; Angeli, C. Metal-to-Metal Charge-Transfer Transitions: Reliable Excitation Energies from Ab Initio Calculations. *Theor. Chem. Acc.* **2012**, *131*, 1−13.
(29) Becke, A. D. Density Functional Thermochemistry. III. The Role of Exact Exchange. *J. Chem. Phys.* **1993**, *98*, 5648−5652.
(30) Becke, A. D. Density-Functional Exchange-Energy Approximation with Correct Asymptotic Behavior. *Phys. Rev. A: At., Mol., Opt. Phys.* **1988**, *38*, 3098−3100.
(31) Lee, C.; Yang, W.; Parr, R. G. Development of the Colle-Salvetti Correlation-Energy Formula into a Functional of the Electron Density. *Phys. Rev. B: Condens. Matter Mater. Phys.* **1988**, *37*, 785−789.
(32) McLean, A. D.; Chandler, G. S. Contracted Gaussian Basis Sets for Molecular Calculations. I. Second Row Atoms, Z=11−18. *J. Chem. Phys.* **1980**, *72*, 5639−5648.
(33) Raghavachari, K.; Trucks, G. W. Highly Correlated Systems. Excitation Energies of First Row Transition Metals Sc-Cu. *J. Chem. Phys.* **1989**, *91*, 1062−1065.
(34) Balabanov, N. B.; Peterson, K. A. Systematically Convergent Basis Sets for Transition Metals. I. All-Electron Correlation Consistent Basis Sets for the 3d Elements Sc-Zn. *J. Chem. Phys.* **2005**, *123*, 064107.
(35) Woon, D. E.; Dunning, T. H. Gaussian Basis Sets for Use in Correlated Molecular Calculations. III. The Atoms Aluminum through Argon. *J. Chem. Phys.* **1993**, *98*, 1358−1371.
(36) Ishikawa, Y.; Vilkas, M. J. Relativistic Quantum Mechanics of Many-electron Systems. *J. Mol. Struct.: THEOCHEM* **2001**, *573*, 139−169.
(37) Reiher, M.; Wolf, A. Exact Decoupling of the Dirac Hamiltonian. II. The Generalized Douglas-Kroll-Hess Transformation up to Arbitrary Order. *J. Chem. Phys.* **2004**, *121*, 10945−10956.
(38) Reiher, M.; Wolf, A. Exact Decoupling of the Dirac Hamiltonian. I. General Theory. *J. Chem. Phys.* **2004**, *121*, 2037−2047.
(39) Neese, F. The ORCA Program System. *WIREs Comput. Mol. Sci.* **2012**, *2*, 73−78.
(40) Valiev, M.; Bylaska, E. J.; Govind, N.; Kowalski, K.; Straatsma, T. P.; Van Dam, H. J. J.; Wang, D.; Nieplocha, J.; Apra, E.; Windus, T. L.; et al. NWChem: A Comprehensive and Scalable Open-Source Solution for Large Scale Molecular Simulations. *Comput. Phys. Commun.* **2010**, *181*, 1477−1489.
(41) Aidas, K.; Angeli, C.; Bak, K. L.; Bakken, V.; Bast, R.; Boman, L.; Christiansen, O.; Cimiraglia, R.; Coriani, S.; Dahle, P.; et al. The Dalton Quantum Chemistry Program System. *WIREs Comput. Mol. Sci.* **2014**, *4*, 269−284.
(42) *Dalton, a Molecular Electronic Structure Program*, Release DALTON2013.0, 2013; see http://daltonprogram.org/.

DOI: 10.1021/acs.jpca.5b02896
J. Phys. Chem. A XXXX, XXX, XXX−XXX